Eur. Phys. J. A **22**, 293–299 (2004)
DOI 10.1140/epja/i2003-10236-6

THE EUROPEAN PHYSICAL JOURNAL A

Energy dependence of the Λ/Σ^0 production cross-section ratio in p-p interactions

P. Kowina[1,5,a], M. Wolke[1], H.-H. Adam[2], A. Budzanowski[3], R. Czyżykiewicz[4], D. Grzonka[1], J. Haidenbauer[1], M. Janusz[4], L. Jarczyk[4], A. Khoukaz[2], K. Kilian[1], P. Moskal[1,4], W. Oelert[1], C. Piskor-Ignatowicz[4], J. Przerwa[4], C. Quentmeier[2], T. Rożek[5], R. Santo[2], G. Schepers[1], T. Sefzick[1], M. Siemaszko[5], J. Smyrski[4], S. Steltenkamp[2], A. Strzałkowski[4], P. Winter[1], P. Wüstner[6], and W. Zipper[5]

[1] Institut für Kernphysik, Forschungszentrum Jülich, D-52425 Jülich, Germany
[2] Institut für Kernphysik, Westfälische Wilhelms-Universität, D-48149 Münster, Germany
[3] Institute of Nuclear Physics, PL-31 342 Cracow, Poland
[4] Institute of Physics, Jagellonian University, PL-30 059 Cracow, Poland
[5] Institute of Physics, University of Silesia, PL-40 007 Katowice, Poland
[6] Zentrallabor für Elektronik, Forschungszentrum Jülich, D-52425 Jülich, Germany

Received: 21 July 2003 / Revised version: 7 May 2004 /
Published online: 3 November 2004 –
Communicated by M. Garçon

Abstract. The production of the Λ- and Σ^0-hyperons has been measured via the $pp \to pK^+\Lambda/\Sigma^0$ reaction at the internal COSY-11 facility in the excess energy range between 14 and 60 MeV. The transition of the Λ/Σ^0 cross-section ratio from about 28 at $Q \leq 13$ MeV to the high-energy level of about 2.5 is covered by the data showing a strong decrease of the ratio between 10 and 20 MeV excess energy. Effects from the final-state interactions in the p-Σ^0 channel seem to be much smaller than in the p-Λ channel. Estimates of the effective range parameters are given for the $N\Lambda$ and the $N\Sigma$ systems.

PACS. 13.75.-n Hadron-induced low- and intermediate-energy reactions and scattering (energy $\leq$ 10 GeV) – 13.75.Ev Hyperon-nucleon interactions – 13.85.Lg Total cross-sections – 25.40.Ep Inelastic proton scattering

1 Introduction

In the kinematical threshold region the strangeness production is commonly described by both non-strange and strange meson exchange with or without explicit inclusion of an intermediate resonance as depicted in the four graphs of fig. 1. While the exchange of the lightest mesons, namely π and K^+, is expected to be dominant in the Λ and Σ^0 production [1–7] there could also be a contribution arising from the exchange of heavier non-strange or strange mesons [8–11]. In addition, proton-hyperon final-state interactions (FSI) play an important role when comparing the $pK^+\Lambda$ and $pK^+\Sigma^0$ reaction channels.

Since the quark structures of the two neutral Λ and Σ^0 hyperons are similar, one can expect similar production mechanisms. In such a case the cross-section ratio $\mathcal{R}_{\Lambda/\Sigma^0} \equiv \frac{\sigma(pp\to pK^+\Lambda)}{\sigma(pp\to pK^+\Sigma^0)}$ should be mainly determined by the isospin relation which leads to $\mathcal{R}_{\Lambda/\Sigma^0} \sim 3$, in good agreement with the value $\mathcal{R}_{\Lambda/\Sigma^0} \approx 2.5$ observed in proton-proton scattering experiments at excess energies $Q \geq 300$ MeV [12]. It is interesting to note that a comparable cross-section ratio was determined in antiproton-proton annihilation experiments leading to $\bar{\Lambda}$-Λ, $\bar{\Sigma}^0$-Λ + c.c. and $\bar{\Sigma}^{\pm}$-$\Sigma^{\mp}$ as performed by the PS185 collaboration at LEAR [13,14].

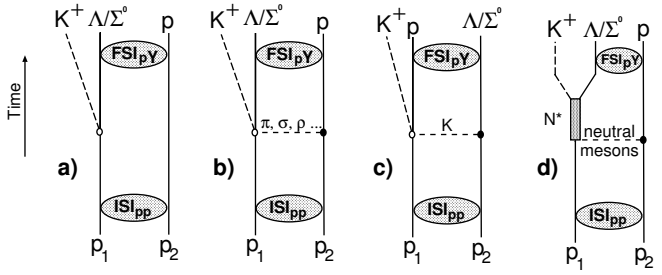

Fig. 1. Examples of possible graphs for the Λ- or Σ^0-hyperon production with inclusion of proton-proton initial (ISI) and proton-hyperon final-state interactions (FSI).

[a] e-mail: p.kowina@fz-juelich.de

Contrary to these results, close-to-threshold data [15] (*i.e.* $Q \leq 13\,\mathrm{MeV}$) taken at the COSY-11 facility [16,17] revealed a ratio of $\mathcal{R}_{\Lambda/\Sigma^0} \approx 28$ as the most remarkable characteristic.

At first a dominant K-exchange mechanism was discussed [15] as a possible explanation of the large Λ/Σ^0 cross-section ratio, which can be determined by the ratio of the squared coupling constants $g^2_{\Lambda NK}/g^2_{\Sigma NK}$, assuming that all other components in the Λ and Σ^0 production diagrams are the same and when neglecting any final-state interactions. It is particularly interesting to note that the ratio of the coupling constants within the $SU(6)$ representation [18,19] leads to $\mathcal{R}_{\Lambda/\Sigma^0} = 27$, which exactly reproduces the experimental result very close to threshold but fails to explain the cross-section ratio observed at high excess energies. In reality it is expected that also π-exchange contributes significantly in the production process. For a review of that issue the reader is referred to [20].

The first COSY-11 data on the ratio encouraged several groups to explain the experimental results. For example calculations within a meson exchange model [7] taking into account pion and kaon exchange (graphs b) and c) in fig. 1) and their interference reproduce the measured excitation functions of Λ and Σ^0 production: while the Λ production channel appears to be dominated by the K exchange mechanism, both π and K exchange contribute with equal strength to the Σ^0 production. Therefore a π-K interference becomes significant only in the Σ^0 case. Indeed the authors of ref. [7] argue that the data require — independent of the hyperon-nucleon potential used for the description of the low-energy final-state scattering process — a destructive interference between the π and K exchange contributions.

Other recent models [5,6,10,11] describe the ratio $\mathcal{R}$ within a factor of two by including heavier exchange mesons (graph b) fig. 1) or nucleon resonances (graph d) fig. 1).

More data were needed to differentiate between the various descriptions and to develop a suitable model for the hyperon production. Therefore, additional cross-sections were measured at the COSY-11 facility in order to determine the energy dependence of the Λ/Σ^0 cross-section ratio in the transition region from $Q \approx 14\,\mathrm{MeV}$ to $Q \approx 60\,\mathrm{MeV}$ where the production ratio changes most drastically.

2 Experiment

The present hyperon (Y) production experiments were performed at the *Co*oler *Sy*nchrotron COSY-Jülich [21] using the COSY-11 detection facility [16,17] shown in fig. 2.

One of the regular COSY dipole magnets serves as a magnetic spectrometer with a H_2 cluster beam target [22] installed in front of it. Due to the advantage of internal beam experiments to use targets with comparatively low areal densities ($\sim 5 \cdot 10^{13}$ atoms/cm^3), energy losses and secondary reactions in the target are negligible. The interaction between a proton of the beam with a proton of the cluster target may lead to the production of neutral hyperons (Σ^0, Λ) via the reactions $pp \to pK^+\Lambda(\Sigma^0)$.

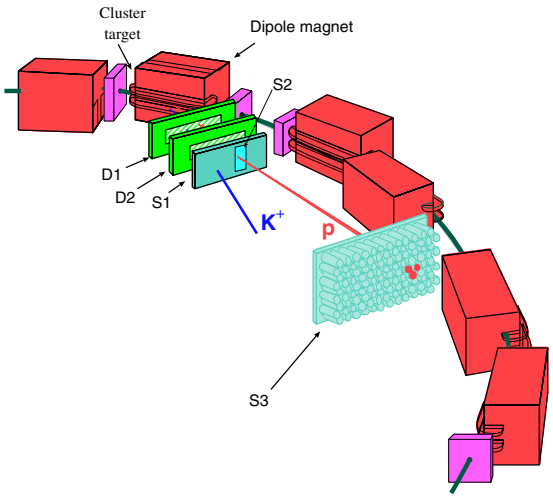

Fig. 2. COSY-11 detection facility.

The selection of $pK^+\Lambda(\Sigma^0)$ events is done by the detection of both positively charged particles in the exit channel (*i.e.* proton and K^+) while the unobserved neutral particle is identified via the missing mass method.

Positively charged ejectiles from these reactions have smaller momenta than the protons in the beam and therefore, they are directed from the circulating beam by the magnetic field of the dipole towards the inner part of the COSY ring.

Leaving the vacuum chamber through a very thin exit foil (300 μm carbon fibre/30 μm Al) [16], the charged reaction products are registered in a set of two drift chambers D1 and D2 for the track reconstruction. With the well-known magnetic field, their momenta can be determined by tracking back to the interaction point. Furthermore, a time-of-flight measurement between the S1(S2) start and the S3 stop scintillator hodoscopes allows to determine their velocity. Therefore, the four-momentum vectors for all positively charged particles can be established and together with the known initial kinematics, the four-momentum of the unobserved neutral hyperon is uniquely determined.

To avoid systematic uncertainties as much as possible, COSY was operated in the "supercycle mode", *i.e.* the beam momenta were changed between the cycles, such that for example 10 cycles with a beam momentum corresponding to the excess energy $Q = 20$ MeV above the Σ^0 threshold were followed by one cycle with the same Q above the Λ production threshold. The ratio of the number of the cycles was chosen inverse to the ratio of the cross-sections for the Λ and Σ^0 production based on the expectations from previous experiments. Thus, both cross-sections were measured under the same conditions and possible changes in the detection system did not influence the data-taking procedure, especially for the determination of the cross-section ratio.

In fig. 3 typical missing-mass spectra for the threshold production of Λ- and Σ^0-hyperons are given, both

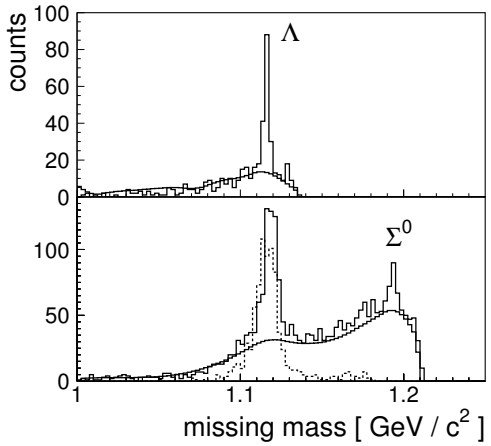

Fig. 3. Spectra of the missing mass for the $pp \to pK^+\Lambda$ (upper part) and $pp \to pK^+\Sigma^0$ (lower part) reactions measured at the same excess energy $Q = 20$ MeV above the Λ and Σ^0 threshold, respectively.

measured at the same excess energy of $Q = 20$ MeV. It is obvious that the peak-to-background ratio is much larger for the Λ than for the Σ^0 production. The solid lines are background distributions as derived from the experimental data themselves by selecting side bands of the two-dimensional invariant *vs.* missing-mass representation below and above the kaon range as described in a previous publication [15]. The small excess of counting rate in the lower part of the figure at smaller missing masses than the Σ^0 peak is due to $pp \to pK^+\Lambda\gamma$ and $pp \to pK^+\Lambda$ reactions with subsequent Λ decay and misidentification of the primary and secondary protons. The dashed line in the lower panel of fig. 3 shows the distribution for the $pp \to pK^+\Lambda$ reaction obtained in Monte Carlo simulations. The background shoulder beyond the Λ peak in the figure for the Σ^0 hyperon production is predominantly due to the decreasing missing-mass resolution with increasing Q value [23]. The background bump below the Λ peak in the lower figure for the Σ^0-hyperon production is due to remaining $pp \to pK^+\Lambda$ events outside the kaon identification cuts; it does not affect the determination of the number of Σ^0 events. To determine this number both background contributions given by the solid and the dashed line were subtracted.

3 Results

3.1 Total cross-section

The total cross-sections extracted for all measured beam momenta are listed in tables 1 and 2 where only the statistical errors are given. In addition, the following systematic uncertainties have to be taken into account: for the background subtraction 15% for Σ^0 and 7% for Λ as well as 3.5% due to the luminosity determination which is performed by a simultaneous measurement of proton-proton elastic scattering [17]. A further systematic error of below 5% is introduced by the detection efficiency which is determined via GEANT [24] simulations assuming an S-wave production process with inclusion of the proton-Y FSI only in the case of the $pp \to pK^+\Lambda$ reaction. The detection efficiencies for different excess energies are shown in tables 1 and 2. The quoted errors on the detection efficiencies of around 4% are due to the statistics of the GEANT simulations which are included in the errors given for the cross-section data.

Table 1. Values of the cross-sections for the Λ production in proton-proton collisions for six excess energies above the production threshold. Only statistical errors are given; for the systematic errors, see text.

$pp \to pK^+\Lambda$		
Excess energy Q (MeV)	Total cross-section σ (nb)	Detection efficiency (%)
13.9 ± 0.5	630 ± 79	0.65 ± 0.02
15.9 ± 0.7	727 ± 57	0.56 ± 0.015
20.2 ± 0.7	1011 ± 99	0.39 ± 0.01
30.1 ± 0.5	1366 ± 247	0.25 ± 0.01
39.7 ± 1.1	2118 ± 266	0.145 ± 0.005
59.3 ± 0.5	3838 ± 624	0.075 ± 0.005

Table 2. Values of the cross-sections for the Σ^0 production in proton-proton collisions for six excess energies above the production threshold. Only statistical errors are given; for the systematic errors, see text.

$pp \to pK^+\Sigma^0$		
Excess energy Q (MeV)	Total cross-section σ (nb)	Detection efficiency (%)
13.8 ± 0.5	34.9 ± 6.5	0.76 ± 0.02
15.9 ± 0.9	46.8 ± 6.4	0.66 ± 0.015
20.3 ± 0.7	78 ± 14	0.47 ± 0.01
29.9 ± 0.5	125 ± 32	0.28 ± 0.01
39.7 ± 1.3	196 ± 33	0.167 ± 0.005
59.1 ± 0.5	482 ± 144	0.078 ± 0.005

To infer the influence of possible higher partial wave contributions, a P-wave in the p-Y system was introduced in the MC simulations. This contribution was estimated from data to be below 20% at a Q value of 60 MeV [25] and much smaller at lower Q values. Partial-wave analyses of the $pp \to pK^+\Lambda$ reaction at a Q-value of 55 MeV are available from COSY-TOF data [25]. Such a P-wave contribution would increase the calculated acceptance by 8%. Therefore, an additional systematic error due to higher partial waves is negligible at the lowest Q-values and may reach 10% at the highest one.

For the Σ^0 channel, the same assumptions of maximal P-wave contribution were made.

In summary, the systematic uncertainties, added linearly, are about 16% to 26% for Λ production, from the lowest to the highest Q-value, and 24% to 34% for Σ^0 production.

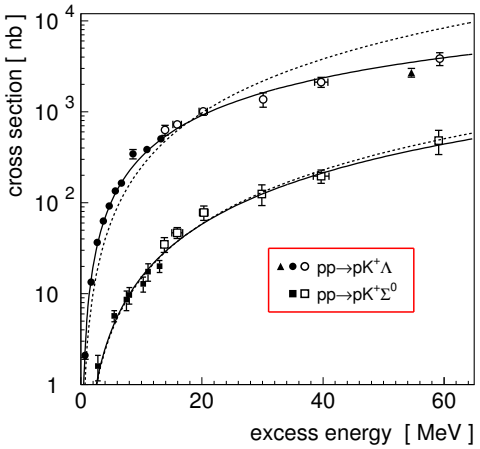

Fig. 4. Total cross-sections for the $pp \to pK^+\Lambda$ and $pp \to pK^+\Sigma^0$ production. Open symbols present results of this work. Full symbols were determined from previous measurements of the COSY-11 [15,26] (circles and squares) and COSY-TOF collaboration [27] (triangle). The plotted error bars include only statistical errors.

Previous COSY-11 measurements of the excitation function for the $pp \to pK^+\Lambda$ and $pp \to pK^+\Sigma^0$ reactions at excess energies up to $Q = 13$ MeV above the production threshold are summarized in [15], where it was pointed out that the energy dependence of the cross-section is much better described by a 3-body phase space behaviour modified by the proton-hyperon (p-Y) final-state interaction [1] than by a calculation taking into account pure phase space only. However, it should be emphasized, that in [15] these fits were naturally limited to the excess energy range of the available data, *i.e.* $Q \leq 13$ MeV.

In fig. 4 the first COSY-11 data [15,26] and one data point obtained by the COSY-TOF collaboration [27] are now extended by the new results up to $Q = 60$ MeV.

The dashed lines in fig. 4 represent χ^2 fits to the full set of data points in the excess energy range $Q \leq 60$ MeV with a pure phase space behaviour [28]:

$$\sigma = K \cdot Q^2, \tag{1}$$

with the normalisation constant K resulting in

$$K(\Lambda) = (3.08 \pm 0.06)\,\mathrm{nb/MeV^2}\,,$$
$$K(\Sigma^0) = (0.150 \pm 0.008)\,\mathrm{nb/MeV^2}\,.$$

The solid lines in fig. 4 are χ^2 fits by the Fäldt and Wilkin parametrisation [1] with inclusion of the energy-dependent flux factor F which accounts for the different kinematics [20]

$$\sigma = \mathrm{const} \cdot \frac{V_{\mathrm{ps}}}{F} \cdot \frac{1}{\left(1 + \sqrt{1 + \frac{Q}{\epsilon'}}\right)^2}$$
$$= C' \cdot \frac{Q^2}{\sqrt{\lambda(s, m_p^2, m_p^2)}} \cdot \frac{1}{\left(1 + \sqrt{1 + \frac{Q}{\epsilon'}}\right)^2}\,. \tag{2}$$

The phase space volume V_{ps} and the flux factor F are given by [28]

$$V_{\mathrm{ps}} = \frac{\pi^3}{2} \frac{\sqrt{m_p\, m_{K^+}\, m_Y}}{(m_p + m_{K^+} + m_Y)^{\frac{3}{2}}}\, Q^2, \tag{3}$$

$$F = 2\,(2\pi)^5 \sqrt{\lambda(s, m_p^2, m_p^2)}. \tag{4}$$

The triangle function λ is defined, *e.g.*, in [28]. The parameter ϵ', which is related to the strength of the p-Y final-state interaction, and the normalisation constant C' are determined by the χ^2 fits for each reaction separately resulting in

$$C'(\Lambda) = (98.2 \pm 3.7)\ \mathrm{nb/MeV^2},$$
$$\epsilon'(\Lambda) = (5.51\,^{+0.58}_{-0.52})\ \mathrm{MeV},$$
$$C'(\Sigma^0) = (2.97\,^{+0.33}_{-0.27}\ \mathrm{nb/MeV^2},$$
$$\epsilon'(\Sigma^0) = (133\,^{+\infty}_{-88})\ \mathrm{MeV}.$$

In case of the Λ production the χ^2-value for the fit is $\chi^2 = 1.8$, which demonstrates a much better description of the data than by pure phase space representation with $\chi^2 = 27$.

On the contrary, in the case of Σ^0 production there is almost no difference between the fit results assuming phase space either with or without FSI, resulting in $\chi^2 = 1.12$ and $\chi^2 = 1.11$, respectively. This might indicate a rather weak p-Σ^0 FSI[1] although this could be also feigned by either higher partial-wave contributions or an energy dependence of the elementary amplitude [29].

Having extracted ϵ' from the fit to the data it is possible to express the results in terms of the averaged effective-range parameters, namely the scattering length $\hat{a}$ and the effective range $\hat{r}$. Assuming only S-wave production, the p-$\Lambda(\Sigma^0)$ systems can be described using the Bargmann potentials [30], where $\hat{a}$ and $\hat{r}$ are expressed as

$$\hat{a} = \frac{\alpha + \beta}{\alpha\beta}\,, \qquad \hat{r} = \frac{2}{\alpha + \beta}\,. \tag{5}$$

While β is a shape parameter, the value of α is calculated via $\epsilon' = \alpha^2/2\mu$, where μ is the reduced mass of the (p-Y) system [30]. The sign of α is ambiguous but the negative value is chosen since (at least for p-Λ) an attractive interaction is expected [31,32].

As can be seen from eq. (5) the parameters $\hat{a}$ and $\hat{r}$ are interdependent and only a deduction of the correlations between them is possible. The extracted correlations for the p-Σ^0 where only a lower bound can be given and p-Λ systems are presented in fig. 5 by solid and dashed lines, respectively. The error ranges (thinner lines) result from the errors in ϵ'.

The results obtained for the p-Λ system are consistent with the value of the spin-averaged parameters determined experimentally [33] and represented in fig. 5 by the cross. In the p-Σ^0 system, the scattering length seems

[1] With $\epsilon' \to \infty$ in eq. (2) neglecting the s dependence in the λ-function one obtains the pure phase space distribution given by eq. (1).

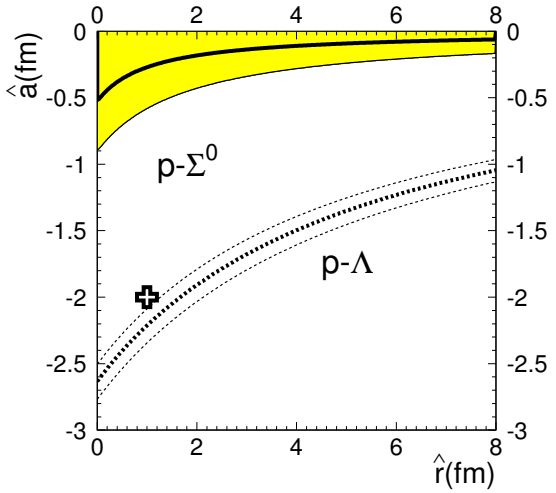

Fig. 5. Correlation between the p-Σ^0 (solid lines for the lower bound) and p-Λ (dashed lines) effective-range parameters obtained as described in the text from $\epsilon(\Sigma^0)$ and $\epsilon(\Lambda)$, respectively. The cross symbol represents the averaged value of the p-Λ effective-range parameters extracted from a FSI approach in threshold Λ production [33].

Table 3. Cross-section ratios for the Λ/Σ^0 productions at six excess energies.

Excess energy Q (MeV)	$\frac{\sigma(pp \to pK^+\Lambda)}{\sigma(pp \to pK^+\Sigma^0)}$
13.9±0.6	18.1 ± 4.1
15.9±0.8	15.5 ± 2.4
20.3±0.8	13.0 ± 2.6
30.0±0.7	10.9 ± 3.4
39.7±1.2	10.8 ± 2.3
59.2±0.7	8.0 ± 2.7

to be much smaller. However, one should be cautious with the interpretation of the result for p-Σ^0. Because of possible transitions in the final state (like $n\Sigma^+ \to p\Sigma^0$) the use of the Fäldt and Wilkin parametrisation allows only to obtain a qualitative estimation of the FSI effects induced by the N-Σ interaction but not directly on the p-Σ^0 channel.

3.2 Energy dependence of the Λ/Σ^0 cross-section ratio

The cross-section ratios for the excess energy range 14 MeV $\leq Q \leq$ 60 MeV are listed in table 3 (and graphically presented in fig. 6), where only statistical errors of the ratios are given.

The data show a strong decrease of the Λ/Σ^0 production ratio in the excess energy range from $\sim$ 10 MeV to $\sim$ 20 MeV. Above 20 MeV the slope is much smaller and the ratio seems to approach slowly the high-energy level.

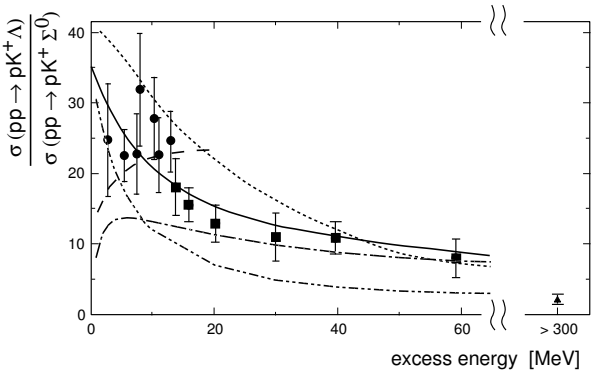

Fig. 6. Energy dependence of the cross-section ratio for Λ/Σ^0 production in proton-proton collisions. Circles and squares present the experimental data from [15] and the present work, respectively. The data point at $Q \geq 300$ MeV is an average taken from the compilation of ref. [12]. The curves represent calculations within different models, π and K exchange with destructive interference [29] (dashed line), incoherent π and K exchange [10] (dashed-dotted), meson exchange with intermediate N^* excitation [10] (dash–double-dotted line) and effective Lagrangian approach including N^* excitation [11] (dotted line). The solid line presents the ratio of the fit functions given by formula 2 and shown in fig. 4.

4 Comparison with model expectations

Within different meson exchange models attempts have been made to reproduce the behavior of the Λ/Σ cross-section ratio, the high threshold value as well as the energy dependence.

A strong $\Sigma N \to \Lambda p$ final-state conversion [15] is rather excluded as a dominant origin of the observed Σ^0 suppression — at least according to a coupled-channel calculation of the Jülich group [7], where both π and K exchange are taken into account with inclusion of the final-state interaction (FSI) effects. Here Λ production is dominated [7] by kaon exchange, which is in line with the experimental results obtained by the DISTO collaboration [34] at higher excess energies (Q = 430 MeV), where the importance of K exchange is confirmed by a measurement of the polarisation transfer coefficient. On the contrary, in the case of Σ^0 production both π and K exchange are found to contribute with about the same strength [7].

A destructive interference of the π and K exchange, suggested by Gasparian *et al.* [7,29], is able to describe the large cross-section ratio close to threshold. Contributions from direct production as well as from heavy-meson exchange were not considered in these calculations but might have an influence on the ratio of the Λ/Σ^0 production as suggested in refs. [8,9,35].

In fig. 6 the energy dependence of the cross-section ratio given by the different models is shown together with the available data. The predictions of the different models are of comparable quality even though different production mechanisms are considered. However, none of them reproduces the data really well.

Studies of the production ratio in ref. [10] consider two different models: The first one is based on π and K

exchange calculations neglecting completely any interferences of the amplitudes [36] (dash-dotted line). The second one considers the exchange of π or heavier mesons with an excitation of intermediate N^*-resonances coupled to the K^+Y channel [8,9] (dash–double-dotted line). Again, any interference of the amplitudes are neglected.

The resonance production is also taken into account in an effective Lagrangian approach [11] (dotted line) based on methods discussed in refs. [37–39], where the strangeness production mechanism is modeled by the exchange of π-, ρ-, ω- and σ-mesons with a subsequent excitation of the nucleon resonances $N^*(1650)$, $N^*(1710)$ and $N^*(1720)$. In those calculations the experimental data are reproduced within a factor of two.

The one-boson exchange calculation performed by Laget [5,6] takes interference effects of pion and kaon exchanges into account by selecting the relative sign for these two mechanism which gives the best description of the cross-sections. The results of those calculations not only reproduce the threshold data of the Λ/Σ^0 ratio within a factor of two and the polarisation transfer results of the DISTO experiment [34] but also describe the missing mass distribution obtained in the inclusive K^+ production measurements performed at SATURNE [40]. However, since the predicted ratio is given only in the excess energy range 4.5 MeV $\leq Q \leq$ 16 MeV [5,6], the results are not shown in fig. 6.

The solid line in fig. 6 results for the ratio of the fit functions as shown in fig. 4 which suggests that the energy dependence is simply governed by the different strengths of the p-Y final-state interactions.

5 Conclusion

At the internal hydrogen cluster target facility COSY-11 the energy dependence of the total cross-sections for the $pp \to pK^+\Lambda$ and $pp \to pK^+\Sigma^0$ production was measured in the range of excess energies between 14 and 60 MeV in order to investigate the transition of the Λ/Σ^0 cross-section ratio $\mathcal{R}$ from $\mathcal{R} \approx 28$ at $Q \leq 13$ MeV to $\mathcal{R} \approx 2.5$ at $Q > 300$ MeV.

A strong decrease of the cross-section ratio in the excess energy range between 10 and 20 MeV is observed. Various models are able to describe the data within a factor of two with comparable quality, even though they differ in the dominant contribution to the production mechanism.

Below $Q = 13$ MeV the measured excitation functions were consistent with comparable final-state interaction strengths in both channels, p-Λ and p-Σ^0 [15]. The new data suggest much weaker final-state interactions in the p-Σ^0 channel than in the case of p-Λ, at least as far as the present results are not feigned by contributions from higher partial waves and/or an energy dependence of the elementary production amplitude.

A measurement with high statistics at an excess energy of 40 MeV $\leq Q \leq$ 60 MeV is highly desirable to study the angular distribution of the produced Λ- and Σ^0-hyperons. This would allow to determine whether higher partial waves already contribute in this energy range. Also, for a significant improvement of the accuracy of the information extracted from the YN FSI a measurement of the corresponding invariant-mass spectra would be very useful [41].

In addition, data with polarized beam and hyperon polarization will be helpful to disentangle the contributing exchange mesons. Also other isospin channels have to be considered. Calculations within the Jülich meson exchange model [7] for other Σ channels have shown that, *e.g.*, the reaction channel $pp \to nK^+\Sigma^+$ is strongly dependent on the π-K interference. For a destructive interference the cross-section for $pp \to nK^+\Sigma^+$ is expected to be a factor of three higher and for constructive interference a factor of three lower than the cross-section for $pp \to pK^+\Sigma^0$.

Data of the reaction $pp \to nK^+\Sigma^+$ have already been taken [42] at COSY-11 and the analysis is in progress.

This work has been supported by the International Büro and the Verbundforschung of the BMBF, the Polish State Committee for Scientific Research, the FFE grants from the Forschungszentrum Jülich and the European Community —Access to Research Infrastructure action of the Improving Human Potential Programme.

References

1. G. Fäldt, C. Wilkin, Z. Phys. A **357**, 241 (1997).
2. G.Q. Li, C.M. Ko, Nucl. Phys. A **594**, 439 (1995).
3. G.Q. Li, C.M. Ko, W.S. Chung, Phys. Rev. C **57**, 434 (1998).
4. A. Sibirtsev, W. Cassing, e-Print Archive (1998), nucl-th/9802019.
5. J.M. Laget, Phys. Lett. B **259**, 24 (1991).
6. J.M. Laget, Nucl. Phys. A **691**, 11 (2001).
7. A. Gasparian *et al.*, Phys. Lett. B **480**, 273 (2000).
8. K. Tsushima, A. Sibirtsev, A.W. Thomas, Phys. Lett. B **390**, 29 (1997).
9. K. Tsushima, A. Sibirtsev, A.W. Thomas, Phys. Rev. C **59**, 369 (1999); **61**, 029903 (2000)(E).
10. A. Sibirtsev *et al.*, e-Print Archive (2000), nucl-th/0004022.
11. R. Shyam, G. Penner, U. Mosel, Phys. Rev. C **63**, 022202 (2001).
12. A. Baldini *et al.*, *Total Cross-Sections for Reactions of High-Energy Particles* Landolt-Börnstein New Ser., Vol. **I/12** (Springer, Berlin, 1988).
13. P. Barnes *et al.*, Phys. Rev. C **54**, 2831 (1996).
14. P. Barnes *et al.*, Phys. Lett. B **402**, 227 (1997).
15. S. Sewerin *et al.*, Phys. Rev. Lett. **83**, 682 (1999).
16. S. Brauksiepe *et al.*, Nucl. Instrum. Methods A **376**, 397 (1996).
17. P. Moskal *et al.*, Nucl. Instrum. Methods A **466**, 448 (2001).
18. J.J. de Swart, Rev. Mod. Phys. **35**, 916 (1963).
19. C.B. Dover, A. Gal, Prog. Part. Nucl. Phys. **12**, 171 (1984).
20. P. Moskal *et al.*, Prog. Part. Nucl. Phys. **49**, 1 (2002).
21. R. Maier, Nucl. Instrum. Methods A **390**, 1 (1997).
22. H. Dombrowski *et al.*, Nucl. Instrum. Methods A **386**, 228 (1997).

23. J. Smyrski *et al.*, Phys. Lett. B **474**, 182 (2000).
24. GEANT-Detector Description and Simulation Tool, CERN Program Library Long Writeup W5013, CERN (1993).
25. A. Metzger, PhD thesis, Universität Erlangen-Nürnberg (1998).
26. J. Balewski *et al.*, Phys. Lett. B **420**, 211 (1998).
27. A. Bilger *et al.*, Phys. Lett. B **420**, 217 (1998).
28. E. Byckling, K. Kajantie, *Particle Kinematics* (John Wiley & Sons Ltd., 1973).
29. A. Gasparyan *et al.*, Schr. FZ-Jülich: Matter Mater. **11**, 205 (2002).
30. R.G. Newton, *Scattering Theory of Waves and Particles* (Springer-Verlag, New York, 1982).
31. B. Holzenkamp, K. Holinde, J. Speth, Nucl. Phys. A **500**, 485 (1989).
32. T.A. Rijken, V.G.J. Stoks, Y. Yamamoto, Phys. Rev. C **59**, 21 (1999).
33. J. Balewski *et al.*, Eur. Phys. J. A **2**, 99 (1998).
34. F. Balestra *et al.*, Phys. Rev. Lett. **83**, 1534 (1999).
35. N. Kaiser, Eur. Phys. J. A **5**, 105 (1999).
36. A. Sibirtsev, Phys. Lett. B **359**, 29 (1995).
37. R. Shyam, U. Mosel, Phys. Lett. B **426**, 1 (1998).
38. R. Shyam, Phys. Rev. C **60**, 055213 (1999).
39. A. Engel *et al.*, Nucl. Phys. A **603**, 387 (1996).
40. R. Siebert *et al.*, Nucl. Phys. A **567**, 819 (1994).
41. A. Gasparyan *et al.*, hep-ph/0311116 (2003).
42. T. Rożek, D. Grzonka, COSY Proposal 117 (2002).